

Article

# Hydrodeoxygenation of Benzofuran over Bimetallic Ni-Cu/ $\gamma$ -Al<sub>2</sub>O<sub>3</sub> Catalysts

Tianhan Zhu, Hua Song \*, Feng Li and Yanguang Chen

Provincial Key Laboratory of Oil & Gas Chemical Technology, College of Chemistry & Chemical Engineering, Northeast Petroleum University, Daqing 163318, China; jutython@foxmail.com (T.Z.); lifeng\_dqpi@sina.com (F.L.); ygchen79310@126.com (Y.C.)

\* Correspondence: songhua@nepu.edu.cn; Tel.: +86-0459-6503167; Fax: +86-0459-6506498

Received: 19 December 2019; Accepted: 17 February 2020; Published: 1 March 2020



**Abstract:** Bimetallic Ni<sub>x</sub>Cu<sub>(10-x)</sub>/ $\gamma$ -Al<sub>2</sub>O<sub>3</sub> catalysts (where  $x$  is the mass fraction of Ni) with different Ni/Cu mass ratios were prepared. The catalysts were characterized by X-ray diffractometry, N<sub>2</sub> adsorption–desorption, inductively coupled plasma mass spectrometry, X-ray photoelectron spectroscopy, H<sub>2</sub>-temperature programmed reduction, and transmission electron microscopy. The effect of Ni/Cu mass ratio on benzofuran hydrodeoxygenation was investigated in a fixed-flow reactor. Cu addition improved the NiO reducibility. The strong interaction of Ni and Cu led to the formation of smaller and highly dispersed CuO and NiO species over  $\gamma$ -Al<sub>2</sub>O<sub>3</sub>, which favors an improvement in catalytic activity. Among the as-prepared catalysts, the Ni<sub>5</sub>Cu<sub>5</sub>/ $\gamma$ -Al<sub>2</sub>O<sub>3</sub> showed the highest deoxygenated product yield (79.9%) with an acceptable benzofuran conversion of 95.2%, which increased by 18.3% and 16.9% compared with that of the monometallic Ni/ $\gamma$ -Al<sub>2</sub>O<sub>3</sub> catalyst. A possible reaction network was proposed, which would provide insight into benzofuran hydrodeoxygenation over the Ni<sub>5</sub>Cu<sub>5</sub>/ $\gamma$ -Al<sub>2</sub>O<sub>3</sub> catalyst.

**Keywords:** bimetallic Ni-Cu; hydrodeoxygenation; benzofuran

## 1. Introduction

In recent years, the increasing combustion of fossil fuels has led to a global energy crisis and environmental issues. Renewable and sustainable energy sources have been explored to resolve the problem. Bio-oil appears to be a possible replacement for fossil fuels, which can be derived from biomass via rapid pyrolysis [1]. However, bio-oil that was produced by rapid pyrolysis contains a mass of oxygenated compounds, such as acids, phenolic, esters, alcohols, and furans [2]. The oxygen-containing compounds of bio-oil yield a higher viscosity, thermal instability, and a poor caloric value, which is undesired for further use in internal combustion engines [3]. Various methods for the removal of oxygenated compounds from oxygen-containing compounds have been trialed to improve the bio-oil pyrolysis properties. Catalytic hydrodeoxygenation (HDO) is considered the most efficient and promising technology to upgrade bio-oil [4,5].

The challenge of bio-oil HDO is to obtain a suitable catalyst with an acceptable activity. Extensive effort has been expended to design feasible HDO catalysts. Numerous investigations have focused on sulfide metals [6–9] and noble metal catalysts [10–12]. Despite the high HDO activity, sulfide catalysts will produce undesirable sulfur-containing compounds in the final products. Noble metal catalysts often show a high activity in oxygen-atom removal. Unfortunately, their commercial applications are limited by their high cost. Alternatively, non-noble metal catalysts, and especially transition metals have been investigated extensively and the bimetallic catalysts show acceptable HDO activity.

Zhou et al. [13] reported that the introduction of Co to Ni/ $\gamma$ -Al<sub>2</sub>O<sub>3</sub> could improve the guaiacol HDO activity, which can be attributed to the synergistic effects of Ni and/or Co with  $\gamma$ -Al<sub>2</sub>O<sub>3</sub>. Co

introduction contributed to a decrease in reduction temperature of the metal oxides and better particle dispersion. Leng et al. [14] synthesized a NiFe/ $\gamma$ -Al<sub>2</sub>O<sub>3</sub> catalyst via incipient wetness co-impregnation; the catalyst exhibited an excellent HDO property and the bio-oil heating value was improved from 37.8 to 43.9 MJ/kg after the catalytic HDO process. Cheng et al. [15] investigated the effect of bimetallic Fe-Co/SiO<sub>2</sub> catalysts on the HDO of pine sawdust bio-oil, which demonstrated that the bimetallic catalysts had a better HDO performance compared with monometallic Fe/SiO<sub>2</sub> or Co/SiO<sub>2</sub> catalysts because of the synergistic effect of Fe and Co. The effect of transition-metal Cu on monometallic catalysts, such as Ni/SBA-15, was also studied because it can decrease the metal-oxide reduction temperature and contribute to the formation of small crystallites of Ni sites in the Ni/SBA-15 catalyst [16]. Tuan et al. [17] found that Cu addition improved the Ni dispersion and contributed to a decrease in Ni reduction temperature. Thus, the Cu provided the Ni-Cu/Al<sub>2</sub>O<sub>3</sub> catalyst with a more desirable catalytic performance in the steam reforming of gasoline than the Ni/Al<sub>2</sub>O<sub>3</sub> catalyst. The non-noble bimetallic Ni-Cu/ $\gamma$ -Al<sub>2</sub>O<sub>3</sub> catalyst may be an alternative catalyst for the HDO of bio-oil. However, to the best of our knowledge, no studies have been reported concerning the use of Ni-Cu/ $\gamma$ -Al<sub>2</sub>O<sub>3</sub> as a catalyst for the HDO of benzofuran (BF).

In this work, bimetallic Ni-Cu/ $\gamma$ -Al<sub>2</sub>O<sub>3</sub> catalysts with different Ni/Cu mass ratios were prepared by co-impregnation and the as-prepared catalysts during the HDO of BF were investigated. BF was a suitable model compound because bio-oil obtained by fast pyrolysis contained mainly phenolic and furanic compounds [18–20]. Interestingly, BF has a similar structure to the organosulfur and organonitrogen compounds for hydrodesulfurization and hydrodenitrogenation reactions, which provides a contrast of HDO to hydrogenation [21]. The as-prepared samples were characterized by X-ray diffractometry (XRD), N<sub>2</sub> adsorption–desorption, H<sub>2</sub>-temperature programmed reduction (H<sub>2</sub>-TPR), inductively coupled plasma mass spectrometry (ICP-MS), X-ray photoelectron spectroscopy (XPS), and transmission electron microscopy (TEM) analysis. Cu addition could improve the HDO performance extensively.

## 2. Results and Discussion

### 2.1. X-ray Diffractometry (XRD)

Figure 1 shows the XRD patterns of the fresh and spent Ni<sub>x</sub>Cu<sub>(10-x)</sub>/ $\gamma$ -Al<sub>2</sub>O<sub>3</sub> catalysts. For all samples (Figure 1a,b), the broad peaks at 36.7°, 46.5°, and 66.3° can be attributed to the  $\gamma$ -Al<sub>2</sub>O<sub>3</sub> support according to JCPDS file No. 50-0741. Figure 1a shows that for fresh monometallic Ni/ $\gamma$ -Al<sub>2</sub>O<sub>3</sub>, the peaks at  $2\theta = 37.2^\circ$ ,  $43.3^\circ$ , and  $62.9^\circ$  can be attributed to the NiO phase according to JCPDS No. 47-1049. For fresh monometallic Cu/ $\gamma$ -Al<sub>2</sub>O<sub>3</sub>, the peaks at  $2\theta = 35.2^\circ$ ,  $38.5^\circ$ , and  $48.6^\circ$  can be attributed to the CuO phase according to JCPDS No. 44-0706. For fresh bimetallic Ni<sub>x</sub>Cu<sub>(10-x)</sub>/ $\gamma$ -Al<sub>2</sub>O<sub>3</sub> catalysts, no obvious peaks that were related to NiO and CuO species were detected, which indicates that the metal oxides were small and beyond the XRD detection limit. Therefore, the NiO and CuO species were dispersed homogeneously on the catalyst surface. In Figure 1b, for the spent monometallic Ni/ $\gamma$ -Al<sub>2</sub>O<sub>3</sub>, weak peaks that belong to NiO species were detected, which was similar to the fresh sample, and showed no significant changes in active phase of the catalyst during reaction. However, for the spent monometallic Cu/ $\gamma$ -Al<sub>2</sub>O<sub>3</sub>, the CuO peaks disappeared and metal Cu peaks were visible at 43.3°, 50.4°, and 74.1°, which shows that CuO was reduced to metal Cu during the reaction in hydrogen. The broad peak at 43.3°, which can be attributed to metal Cu, was detected for the spent bimetallic Ni<sub>x</sub>Cu<sub>(10-x)</sub>/ $\gamma$ -Al<sub>2</sub>O<sub>3</sub> catalysts and shows that a reduction of CuO to metal Cu occurred during the reaction. Compared with the spent monometallic Cu/ $\gamma$ -Al<sub>2</sub>O<sub>3</sub>, the peak of metal Cu at 43.3° of the bimetallic Ni<sub>x</sub>Cu<sub>(10-x)</sub>/ $\gamma$ -Al<sub>2</sub>O<sub>3</sub> catalyst was broader, which indicates that the particle size of metal Cu that formed on the bimetallic Ni<sub>x</sub>Cu<sub>(10-x)</sub>/ $\gamma$ -Al<sub>2</sub>O<sub>3</sub> catalyst surface was much smaller. Among the bimetallic Ni<sub>x</sub>Cu<sub>(10-x)</sub>/ $\gamma$ -Al<sub>2</sub>O<sub>3</sub> catalysts, the Ni<sub>5</sub>Cu<sub>5</sub>/ $\gamma$ -Al<sub>2</sub>O<sub>3</sub> showed the highest peak intensity at 43.3°, which indicates the best reducibility of the Ni<sub>5</sub>Cu<sub>5</sub>/ $\gamma$ -Al<sub>2</sub>O<sub>3</sub> catalyst.

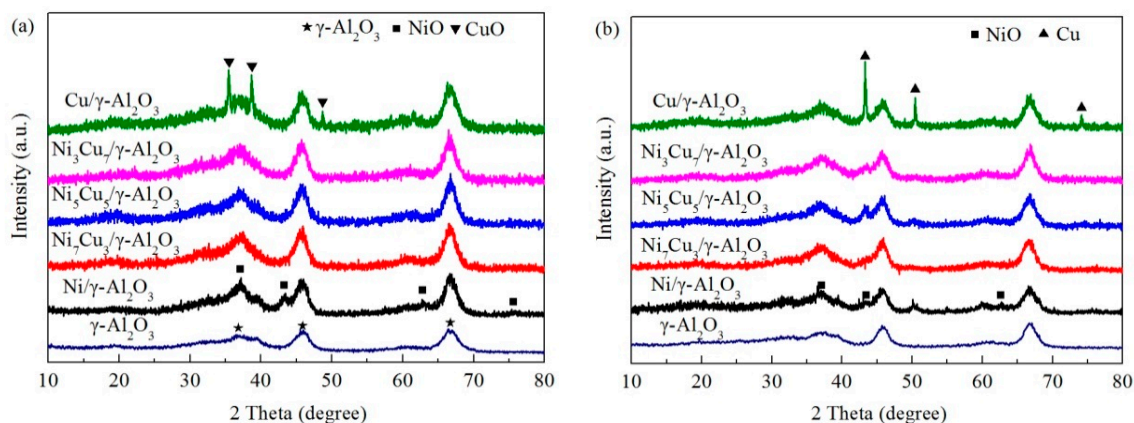


**Figure 1.** X-ray diffractometry (XRD) patterns of (a) fresh and (b) spent  $Ni_xCu_{(10-x)}/\gamma-Al_2O_3$  catalysts.

## 2.2. Brunauer–Emmett–Teller Analysis

Figure 2 shows the  $N_2$  adsorption–desorption isotherms and pore size distributions of the supported  $Ni_xCu_{(10-x)}/\gamma-Al_2O_3$  catalysts. Figure 2a shows that all as-prepared samples displayed a type-IV isotherm with an H1-type hysteresis loop [22], which indicates that all samples maintained the mesoporous structure of the  $\gamma-Al_2O_3$  support. The sample pore size distribution (Figure 2b) with different Ni/Cu mass ratios showed no obvious differences and the average pore diameters were  $\sim 10.0$  nm.

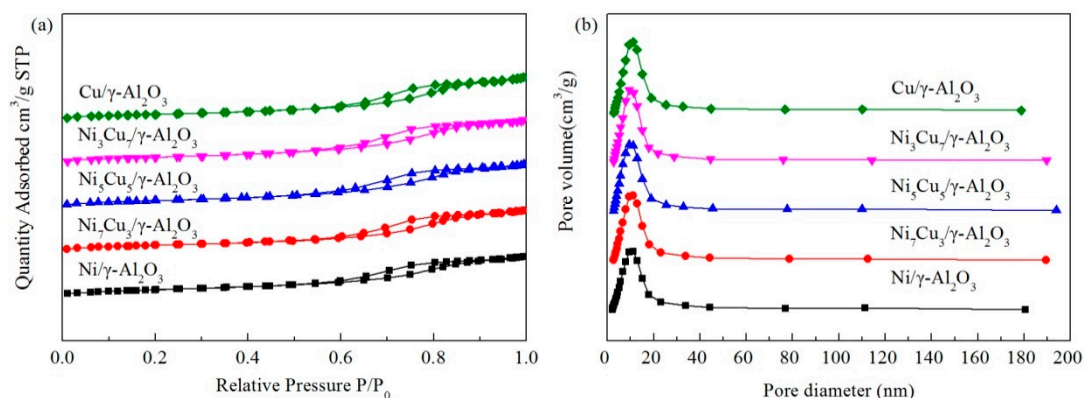


**Figure 2.**  $N_2$  adsorption–desorption isotherms (a) and pore size distributions (b) of the  $Ni_xCu_{(10-x)}/\gamma-Al_2O_3$  catalysts.

Table 1 lists the textural properties of the  $Ni_xCu_{(10-x)}/\gamma-Al_2O_3$  catalysts. The Ni and Cu sample loading was obtained by ICP analysis and is listed in Table 1. The metal loading of various catalysts was close to the nominal values. As shown in Table 1, the specific surface area of the blank  $\gamma-Al_2O_3$  support was  $257\text{ m}^2\cdot\text{g}^{-1}$ , with an average pore diameter of 10.9 nm and a pore volume of  $0.70\text{ cm}^3\cdot\text{g}^{-1}$ , respectively. Upon active metal Ni or/and Cu addition into  $\gamma-Al_2O_3$ , the  $\gamma-Al_2O_3$  specific surface area and volume decreased remarkably. This may result from the blocking of  $\gamma-Al_2O_3$  channels with metal oxides. The specific surface areas of monometallic  $Ni/\gamma-Al_2O_3$  and  $Cu/\gamma-Al_2O_3$  were  $130\text{ m}^2\cdot\text{g}^{-1}$  and  $139\text{ m}^2\cdot\text{g}^{-1}$ , respectively. Compared with the monometallic  $Ni/\gamma-Al_2O_3$  sample, the Cu-doped bimetallic catalysts had a higher specific surface area, especially for  $Ni_5Cu_5/\gamma-Al_2O_3$  ( $153\text{ m}^2\cdot\text{g}^{-1}$ ) and  $Ni_3Cu_7/\gamma-Al_2O_3$  ( $151\text{ m}^2\cdot\text{g}^{-1}$ ). The specific surface area of  $Ni_5Cu_5/\gamma-Al_2O_3$  and  $Ni_3Cu_7/\gamma-Al_2O_3$  is higher than that of  $Cu/\gamma-Al_2O_3$ , which may be explained by the lower pore occlusion from smaller particles. This phenomenon agrees with the subsequent TEM analysis.

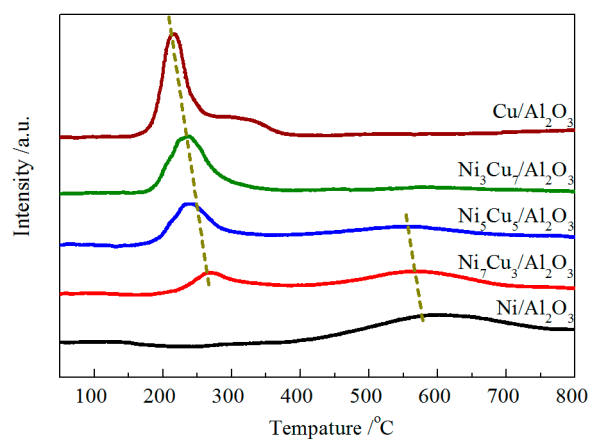
**Table 1.** Chemical composition and textural properties of fresh Ni<sub>x</sub>Cu<sub>(10-x)</sub>/γ-Al<sub>2</sub>O<sub>3</sub> catalysts.

Samples	Actual Loading <sup>a</sup> (wt.%)		BET Surface Area (m <sup>2</sup> ·g <sup>-1</sup> )	Pore Volume (cm <sup>3</sup> ·g <sup>-1</sup> )	Pore Diameter (nm)
	Ni	Cu			
γ-Al <sub>2</sub> O <sub>3</sub>	-	-	257	0.70	10.9
Ni/γ-Al <sub>2</sub> O <sub>3</sub>	8.3	-	130	0.32	8.0
Ni <sub>7</sub> Cu <sub>3</sub> /γ-Al <sub>2</sub> O <sub>3</sub>	5.2	2.9	136	0.33	8.5
Ni <sub>5</sub> Cu <sub>5</sub> /γ-Al <sub>2</sub> O <sub>3</sub>	3.3	4.8	153	0.35	8.2
Ni <sub>3</sub> Cu <sub>7</sub> /γ-Al <sub>2</sub> O <sub>3</sub>	2.4	5.9	151	0.36	8.3
Cu/γ-Al <sub>2</sub> O <sub>3</sub>	-	8.7	139	0.35	9.0

<sup>a</sup> Determined by inductively coupled plasma (ICP) analysis.

### 2.3. H<sub>2</sub>-Temperature Programmed Reduction (H<sub>2</sub>-TPR)

The sample reducibility was investigated by H<sub>2</sub>-TPR, and the spectrum is shown in Figure 3. As shown in Figure 3, the monometallic Ni/γ-Al<sub>2</sub>O<sub>3</sub> showed a broad peak at ~400–750 °C, which was assigned to a reduction of bulk NiO species in the pore structure and NiAl<sub>2</sub>O<sub>4</sub> species from the strong interaction between Ni and Al in high-temperature calcination [13,22]. For Cu/γ-Al<sub>2</sub>O<sub>3</sub>, the main peak centered at 220 °C was attributed to the reduction of CuO to Cu, and a shoulder at ~300 °C was observed, which was assigned to the strong interaction of Cu particles and defective Al<sup>3+</sup> sites [23]. Compared with the monometallic catalysts, two reduction peaks were observed for bimetallic Ni<sub>x</sub>Cu<sub>(10-x)</sub>/γ-Al<sub>2</sub>O<sub>3</sub>; the former that was centered at 230–260 °C was assigned to CuO reduction and the latter centered at 550–580 °C was attributed to a reduction of bulk NiO. The reduction peak shifted to a low temperature with an increase in Cu loading, which indicates that Cu addition could decrease the interaction of the NiO with the support and improve the NiO reducibility [24].

**Figure 3.** H<sub>2</sub>-temperature programmed reduction (H<sub>2</sub>-TPR) profiles of Ni<sub>x</sub>Cu<sub>(10-x)</sub>/γ-Al<sub>2</sub>O<sub>3</sub> catalysts.

### 2.4. X-ray Photoelectron Spectroscopy (XPS)

The chemical states of the fresh and spent catalysts were measured by XPS analysis. For the fresh catalyst, as shown in Figure 4a, the peak of fresh Ni/γ-Al<sub>2</sub>O<sub>3</sub> and bimetallic Ni<sub>5</sub>Cu<sub>5</sub>/γ-Al<sub>2</sub>O<sub>3</sub> catalyst at 855.2–855.5 eV is ascribed to the strong reaction of NiO with γ-Al<sub>2</sub>O<sub>3</sub>. A satellite peak was present at ~862.0 eV [25]. For spent Ni/γ-Al<sub>2</sub>O<sub>3</sub> and bimetallic Ni<sub>x</sub>Cu<sub>(10-x)</sub>/γ-Al<sub>2</sub>O<sub>3</sub> catalysts (Figure 4c), the peak at 856.1–856.3 eV can be ascribed to the strong reaction of NiO with γ-Al<sub>2</sub>O<sub>3</sub>, and a satellite peak appeared at 862.2 eV [26]. Therefore, the Ni species existed mainly as the NiO phase for the fresh and spent Ni/γ-Al<sub>2</sub>O<sub>3</sub> and bimetallic Ni<sub>x</sub>Cu<sub>(10-x)</sub>/γ-Al<sub>2</sub>O<sub>3</sub> catalysts, which agrees with the XRD analysis. For the spent Ni<sub>5</sub>Cu<sub>5</sub>/γ-Al<sub>2</sub>O<sub>3</sub> catalyst, a peak appeared at 856.3 eV, which can be assigned to NiO, and which was slightly higher than that of the monometallic Ni/γ-Al<sub>2</sub>O<sub>3</sub> catalyst (856.1 eV). Hou et al. [25] found that the binding energy was related to the metal particle size, and small particles often displayed higher binding energy values. In our case, the Ni<sub>5</sub>Cu<sub>5</sub>/γ-Al<sub>2</sub>O<sub>3</sub> catalyst possessed the highest binding

energy among the as-prepared samples, which means that the  $\text{Ni}_5\text{Cu}_5/\gamma\text{-Al}_2\text{O}_3$  catalyst provided a better NiO dispersion.

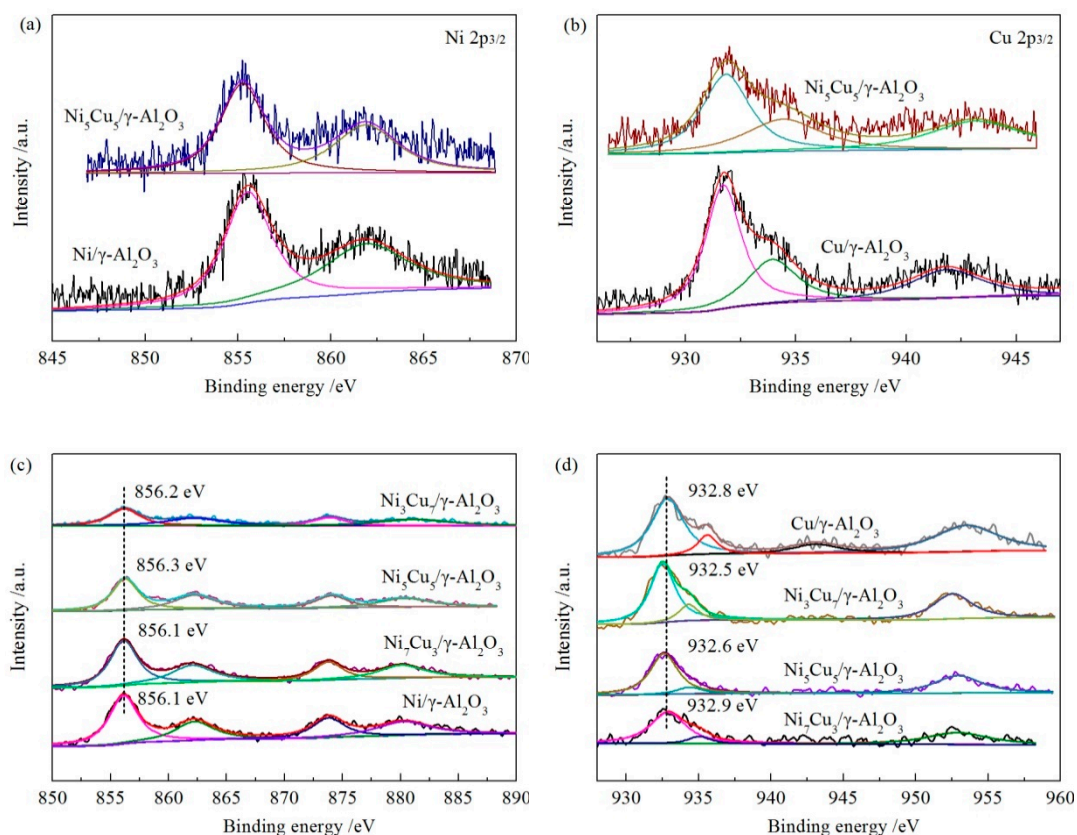


**Figure 4.** X-ray photoelectron spectroscopy (XPS) analysis of the (a,b) fresh and (c,d) spent catalysts: (a,c) Ni 2p; (b,d) Cu 2p.

In Figure 4b, the two characteristic peaks for fresh  $\text{Cu}/\gamma\text{-Al}_2\text{O}_3$  and bimetallic  $\text{Ni}_5\text{Cu}_5/\gamma\text{-Al}_2\text{O}_3$  at 931.7–931.8 eV and 934.1–934.4 eV were assigned to  $\text{Cu}^+$  and  $\text{Cu}^{2+}$ , respectively [27]. In Figure 4d, the spent Cu-based catalysts showed two characteristic peaks, the former at 932.5–932.9 eV was attributed to  $\text{Cu}^0$  or/and  $\text{Cu}^+$  and the latter at 934.3–935.6 eV was assigned to  $\text{Cu}^{2+}$  species [27]. The existence of  $\text{Cu}^0$  was confirmed by XRD analysis, therefore the peak at 932.5–932.9 eV is probably  $\text{Cu}^0$ . For the typical bimetallic  $\text{Ni}_5\text{Cu}_5/\gamma\text{-Al}_2\text{O}_3$ , the Cu 2p<sub>3/2</sub> bonding energy (BE) values (932.6 eV) were lower than those of the monometallic  $\text{Cu}/\gamma\text{-Al}_2\text{O}_3$  catalyst (932.8 eV). This may result from electron transfer from Ni to Cu that is caused by the interaction between Cu and Ni. Xin et al. [28] demonstrated that the addition of a second metal, namely, Co, contributed to electron transfer from Ni to Co, which increased the BE value of the Ni species. Similar results have been reported by Liu et al., [27] who found that the BE value of Ni shifted to a higher value and the Cu shifted to a lower value, because Cu addition contributed to electron transfer from Ni to Cu. This phenomenon demonstrated the interaction of Ni and Cu.

### 2.5. Transmission Electron Microscopy (TEM)

The dispersion of monometallic catalysts ( $\text{Ni}/\gamma\text{-Al}_2\text{O}_3$  and  $\text{Cu}/\gamma\text{-Al}_2\text{O}_3$ ) and bimetallic catalysts was measured by TEM. Figure 5a shows that the active site for the monometallic  $\text{Ni}/\gamma\text{-Al}_2\text{O}_3$  aggregated and formed large particles (dark zone) with a size up to 26 nm. The particle distribution of  $\text{Ni}/\gamma\text{-Al}_2\text{O}_3$  is shown in Figure 5f. The mean diameter was  $\sim 7.90$  nm. With Cu addition, the sizes of active metal sites decreased and their dispersion became more uniform, which shows that the Cu contributed to the formation of small particles with a better dispersion. The  $\text{Ni}_5\text{Cu}_5/\gamma\text{-Al}_2\text{O}_3$  catalyst had a mean

diameter of 4.85 nm, which was much smaller than that of the monometallic Ni/ $\gamma$ -Al<sub>2</sub>O<sub>3</sub>, and indicates the positive effect of Cu addition on the dispersion of metal species. Similar results have been reported by Cai [24]. This behavior may result because Cu addition improves the reducibility of nickel oxide (Figure 3, H<sub>2</sub>-TPR analysis), which led to the formation of smaller active particles. The smaller size and uniformly dispersed metal particles improve the catalytic activity, which will be discussed later. For Cu/ $\gamma$ -Al<sub>2</sub>O<sub>3</sub>, the active metal particle size reached 11 nm, but the dominant size (5.98 nm) was smaller than that of Ni/ $\gamma$ -Al<sub>2</sub>O<sub>3</sub>.

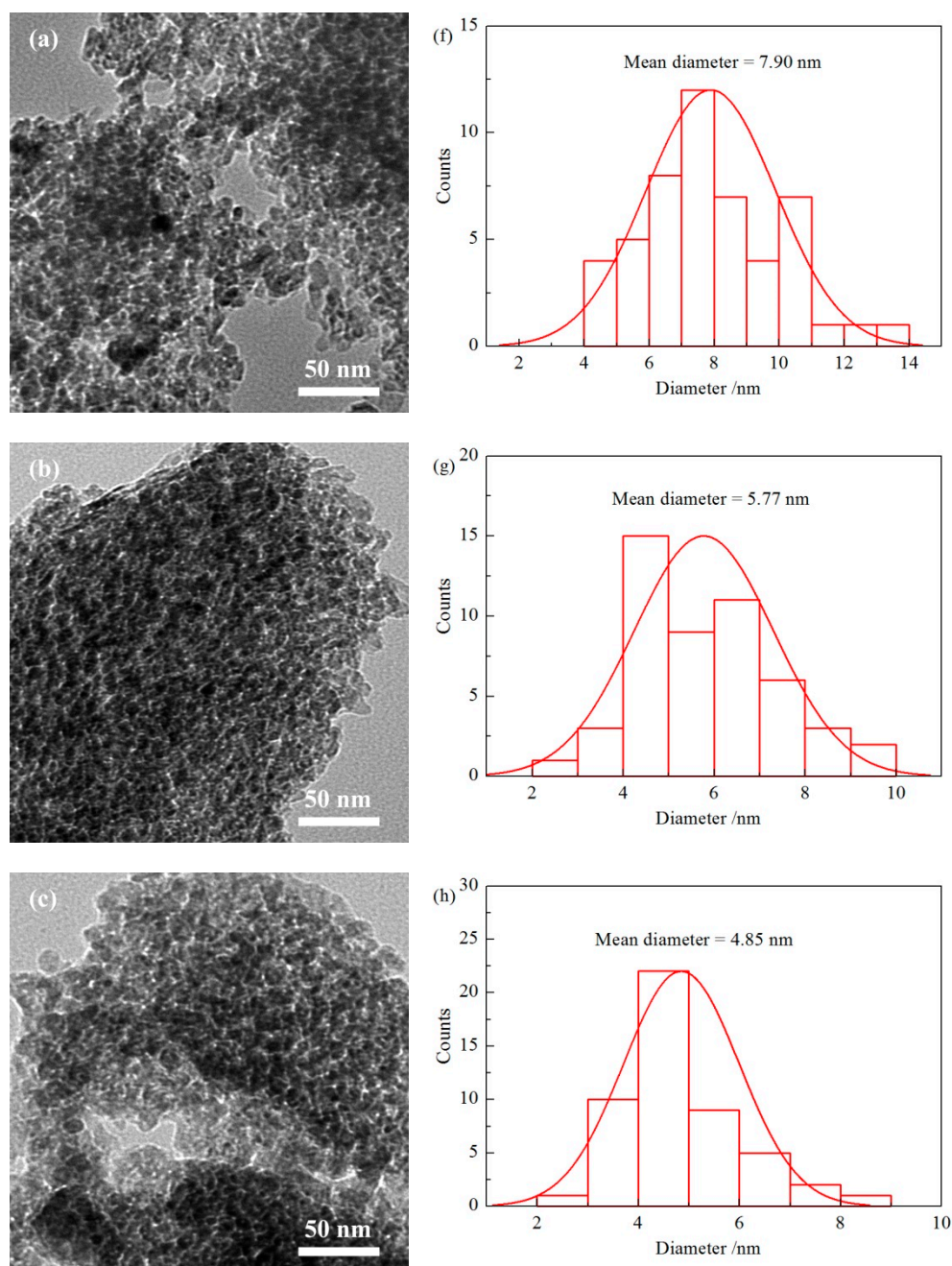
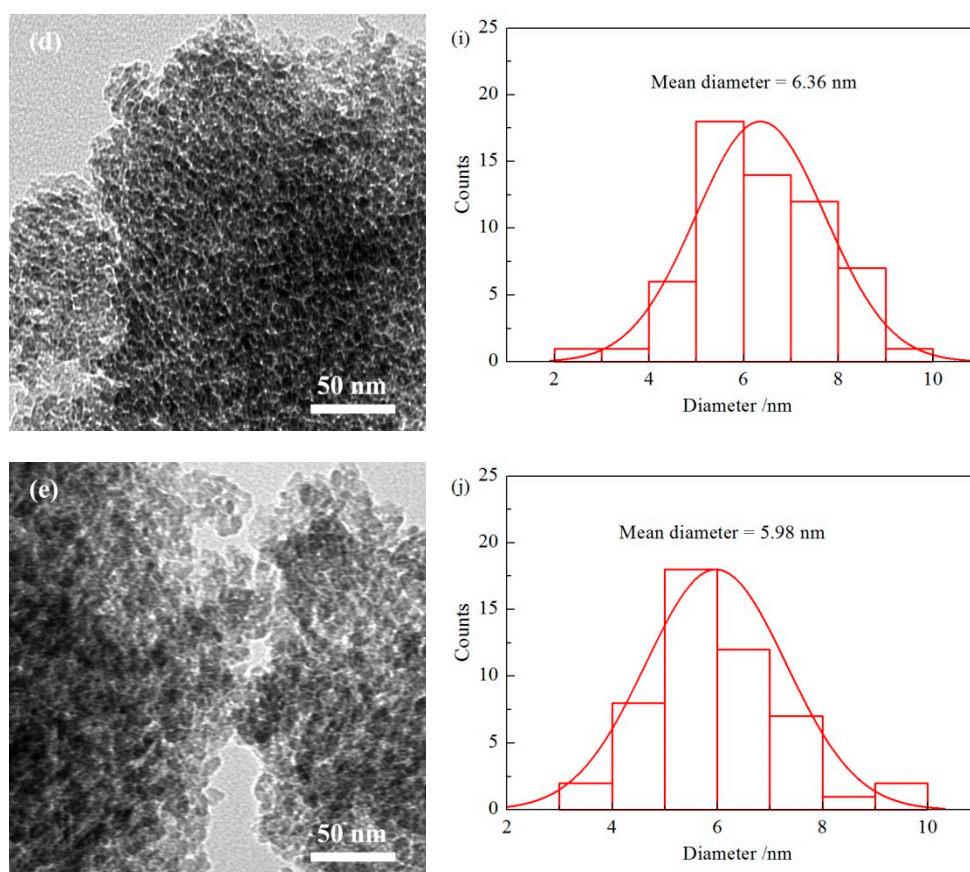


Figure 5. Cont.



**Figure 5.** Transmission electron microscopy (TEM) images and particle distribution of bimetallic  $Ni_xCu_{(10-x)}/\gamma-Al_2O_3$  catalysts. (a,f)  $Ni/\gamma-Al_2O_3$ ; (b,g)  $Ni_7Cu_3/\gamma-Al_2O_3$ ; (c,h)  $Ni_5Cu_5/\gamma-Al_2O_3$ ; (d,i)  $Ni_3Cu_7/\gamma-Al_2O_3$ ; (e,j)  $Cu/\gamma-Al_2O_3$ .

### 2.6. Hydrodeoxygenation (HDO) Performance of Bimetallic $Ni_xCu_{(10-x)}/\gamma-Al_2O_3$ Catalysts

The HDO performance of BF over the as-prepared catalysts was tested at 300 °C and 3.0 MPa of total  $H_2$  pressure for 8 h time on stream. As shown in Figure 6, the initial conversion of BF over  $Ni/\gamma-Al_2O_3$  was ~78.3%, although the maximum conversion reached 84.5%. All Cu-doped catalysts, including monometallic  $Cu/\gamma-Al_2O_3$  and bimetallic  $Ni-Cu/\gamma-Al_2O_3$  showed excellent catalytic activities (> 94.5%), which were higher than that of  $Ni/\gamma-Al_2O_3$ , and indicate that Cu addition can increase the BF HDO activity. The lower HDO activity of  $Ni/\gamma-Al_2O_3$  may result from Ni species aggregation, which led to a decrease in exposed active Ni sites. Cu addition favored the reduction of NiO to Ni ( $H_2$ -TPR analysis), which would promote the formation of more Ni sites. Electron transfer from Ni to Cu (XPS analysis) in the  $Ni-Cu/\gamma-Al_2O_3$  catalysts accelerated the C–O bond cleavage, which contributed to the HDO of BF [29].

To investigate the reaction mechanism of the HDO of BF over the catalysts, the product distributions (8 h) were analyzed and the results are shown in Figure 7. The oxygen-containing chemicals were 2,3-dihydrobenzofuran (2,3-DHBF), 2-ethylphenol (2-EtPh), and phenol (Ph), and the O-free compounds included benzene (B), methylbenzene (MB), ethylbenzene (EB), methylcyclohexane (MCH), and ethylcyclohexane (ECH). For the  $Ni/\gamma-Al_2O_3$  catalyst, the selectivity to Ph was 30.7%, followed by ECH (26.3%), which is much higher than that of other products. The high selectivity to Ph indicates the massive cleavage of C–C bonds. Compared with  $Ni/\gamma-Al_2O_3$ , the selectivity to Ph over  $Cu/\gamma-Al_2O_3$  and  $Ni_xCu_{(10-x)}/\gamma-Al_2O_3$  catalysts decreased, whereas the selectivity to O-free ECH increased significantly. Thus, the desired ECH was the only dominant product. Typically, for  $Ni_5Cu_5/\gamma-Al_2O_3$ , the selectivity to ECH was 72.3%, which was 46% higher than that of monometallic  $Ni/\gamma-Al_2O_3$ . As shown in the TEM analysis, the  $Ni_5Cu_5/\gamma-Al_2O_3$  had the smallest particle size of 4.85 nm, which indicates a uniform

dispersion of active sites. As a result, the better dispersion and decreased particle size contributed to an improved HDO performance, which implied increased hydrogenation and deoxygenation. Yang et al. [30] certified that smaller metal particles improved hydrogenation and deoxygenation. The selectivity to the oxygenated intermediate product Ph decreased to 2.7%. A high selectivity to ECH was desired, because more ECH implies a reservation of high calories for raw materials with a high carbon content [31]. For all as-prepared catalysts, the selectivity to EB was ~10.0%, whereas the selectivity to MB and 2-EtPh was low (<1.5%) and can be neglected.

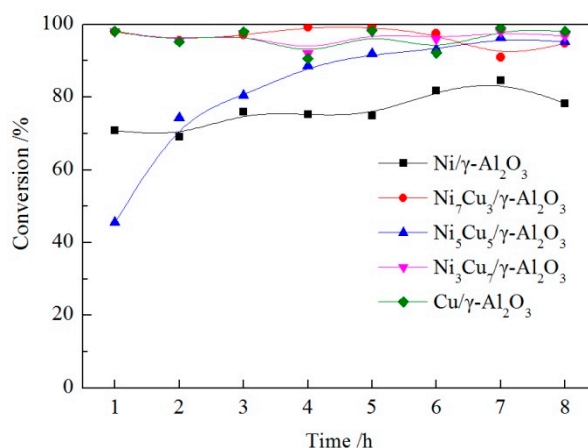


**Figure 6.** Conversion of benzofuran (BF) over  $\text{Ni}_x\text{Cu}_{(10-x)}/\gamma\text{-Al}_2\text{O}_3$  catalysts. (Reaction conditions:  $T = 300\text{ }^\circ\text{C}$ ,  $p = 3.0\text{ MPa}$ ,  $\text{WHSV} = 4.0\text{ h}^{-1}$ , and  $\text{H}_2/\text{oil} = 500\text{ (V/V)}$ ).

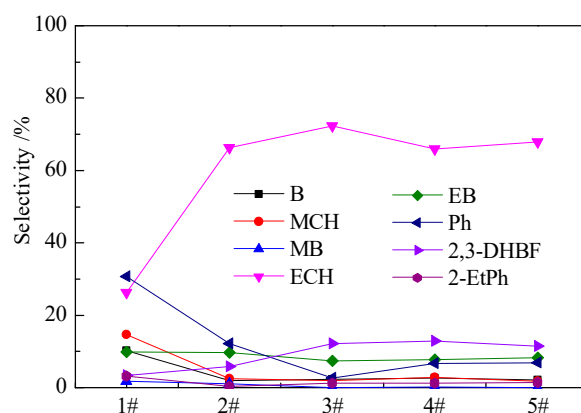
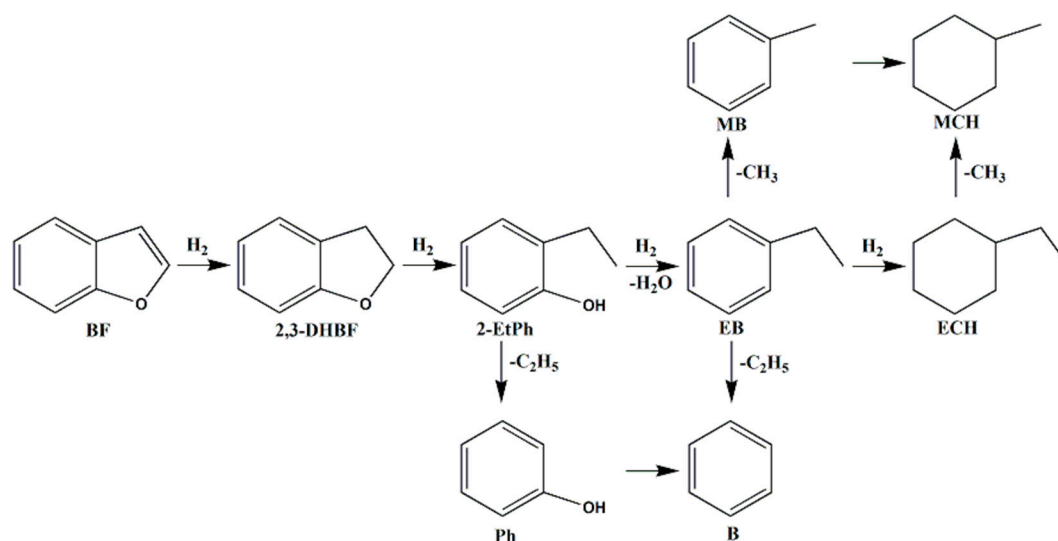


**Figure 7.** Production distribution of  $\text{Ni}_x\text{Cu}_{(10-x)}/\gamma\text{-Al}_2\text{O}_3$  ( $x = 0, 3, 5, 7, 10$ ) catalysts at 8 h (1#- $\text{Ni}/\gamma\text{-Al}_2\text{O}_3$ ; 2#- $\text{Ni}_7\text{Cu}_3/\gamma\text{-Al}_2\text{O}_3$ ; 3#- $\text{Ni}_5\text{Cu}_5/\gamma\text{-Al}_2\text{O}_3$ ; 4#- $\text{Ni}_3\text{Cu}_7/\gamma\text{-Al}_2\text{O}_3$ ; 5#- $\text{Cu}/\gamma\text{-Al}_2\text{O}_3$ ). (Reaction conditions:  $T = 300\text{ }^\circ\text{C}$ ,  $p = 3.0\text{ MPa}$ ,  $\text{WHSV} = 4.0\text{ h}^{-1}$ , and  $\text{H}_2/\text{oil} = 500\text{ (V/V)}$ ).

Based on our previous study [32,33], the proposed reaction network in the HDO of BF over  $\text{Ni}_5\text{Cu}_5/\gamma\text{-Al}_2\text{O}_3$  catalyst is shown in Scheme 1. The 2,3-DHBF was formed initially by hydrogenation and followed by ring opening via C–O bonding cleavage, which was reported to be the key step [34]. Two reaction routes existed for ring-opening of 2-MTHF via the C–O bond cleavage. For BF, it was difficult to break the C–O bond that was linked to the benzene ring owing to the high dissociation energy. Therefore, 2,3-DHBF was converted to 2-EtPh through C–O bond cleavage followed by dehydroxylation and hydrogenation in sequence. The content of decarbonylated products (Ph, B, MB, MCH) was neglected because their selectivities were low, which indicates the slow rate of correlative reactions.



**Scheme 1.** Proposed reaction network for the benzofuran hydrodeoxygenation (BF HDO) over  $\text{Ni}_5\text{Cu}_5/\gamma\text{-Al}_2\text{O}_3$  catalyst [32]. (Reaction conditions:  $T = 300\text{ }^\circ\text{C}$ ,  $p = 3.0\text{ MPa}$ ,  $\text{WHSV} = 4.0\text{ h}^{-1}$ , and  $\text{H}_2/\text{oil} = 500\text{ (V/V)}$ ).

The deoxygenated product yield of bimetallic  $\text{Ni}_x\text{Cu}_{(10-x)}/\gamma\text{-Al}_2\text{O}_3$  catalysts is shown in Figure S1. The HDO product yield of the monometallic  $\text{Ni}/\gamma\text{-Al}_2\text{O}_3$  catalyst was only 61.6%, which was caused by a massive formation of oxygenated compound Ph (shown in Figure 7). With a decrease in Ni/Cu mass ratio, the oxygen-free product yield increased initially, decreased, and reached a maximum of 79.9% at a Ni/Cu mass ratio of 1. Compared with monometallic  $\text{Ni}/\gamma\text{-Al}_2\text{O}_3$  (61.6%) and  $\text{Cu}/\gamma\text{-Al}_2\text{O}_3$  catalysts (74.2%), the yield of oxygen-free compounds of typical  $\text{Ni}_5\text{Cu}_5/\gamma\text{-Al}_2\text{O}_3$  catalysts increased by 18.3% and 5.7%, respectively, which indicates that the bimetallic  $\text{Ni}_5\text{Cu}_5/\gamma\text{-Al}_2\text{O}_3$  catalyst showed a better oxygen removal performance than those of the monometallic catalysts, which favor high-quality bio-oil production (i.e., a high H/C ratio). A low selectivity to ECH meant carbon atom loss via cleavage of the C–C bond during the HDO process. This led to an undesired decrease in heat value of the bio-oil. However, carbon atom retention was desired to maximize the bio-oil quality. Fortunately, a high selectivity to ECH with a high oxygen removal was achieved for bimetallic  $\text{Ni}_x\text{Cu}_{(10-x)}/\gamma\text{-Al}_2\text{O}_3$  catalysts. For  $\text{Ni}_5\text{Cu}_5/\gamma\text{-Al}_2\text{O}_3$ , the maximum ECH selectivity reached 72.3% with an HDO yield of 79.9%, which was much higher than that of monometallic  $\text{Ni}/\gamma\text{-Al}_2\text{O}_3$  (an ECH selectivity of 26.3% with an HDO yield of 61.6%). A comparison of the typical catalytic activity of BF HDO from literature with our results is summarized in Table 2, and has been reported in our previous study [35]. The BF HDO activity of  $\text{Ni}_5\text{Cu}_5/\gamma\text{-Al}_2\text{O}_3$  is higher than that of most reported catalysts.

**Table 2.** Comparison of the typical results of BF HDO from literatures with our present results.

Samples	Temperature (K)	Pressure (MPa)	Conversion (%)	Ref. no.
Sulfided $\text{NiMo}/\text{Al}_2\text{O}_3^a$	553	2.0	74.6	43
Sulfided $\text{NiMo}/\text{Al}_2\text{O}_3^a$	553	5.0	82.5	43
$\text{NiMoP}/\text{Al}_2\text{O}_3^a$	613	7.0	80.7	44
$\text{Pt}/\text{SiO}_2\text{-Al}_2\text{O}_3$	553	3.0	80	45
$\text{Pd}/\text{SiO}_2\text{-Al}_2\text{O}_3$	553	3.0	97	45
$\text{W}_2\text{C}(\text{Ar-2-1023 K-1 h})$	613	4.0	41	46
$\text{Ni}_2\text{P-N}/\text{MCM-41}$	493	3.0	31	40
$\text{Ni}_2\text{P-O}/\text{MCM-41}$	493	3.0	57	40
$\text{Ni}_2\text{P}/\text{Al}_2\text{O}_3$	573	3.0	78	47
$\text{Ni}_2\text{P}/\text{TiO}_2$	573	3.0	85	47
$\text{Ni}_2\text{P}/\text{Al}_2\text{O}_3@\text{TiO}_2$	573	3.0	95	47
$\text{Ni}_5\text{Cu}_5/\gamma\text{-Al}_2\text{O}_3$	573	3.0	95	This work

<sup>a</sup> With  $\text{H}_2\text{S}$  in the feed.

The effect of reaction temperature on HDO performance over a  $\text{Ni}_5\text{Cu}_5/\gamma\text{-Al}_2\text{O}_3$  catalyst has also been investigated. As shown in Figure 8, BF conversion over the  $\text{Ni}_5\text{Cu}_5/\gamma\text{-Al}_2\text{O}_3$  catalyst was 78.0% at 260 °C. The conversion increased to ~95.0% at a higher reaction temperature and was nearly independent of temperature. For the product distribution, the deoxygenated ECH was the predominant product (>65%) for 260–320 °C. The selectivity to EB decreased from 14.9% to 4.4%, which showed that the hydrogenation of EB to ECH was accelerated with an increase in reaction temperature.

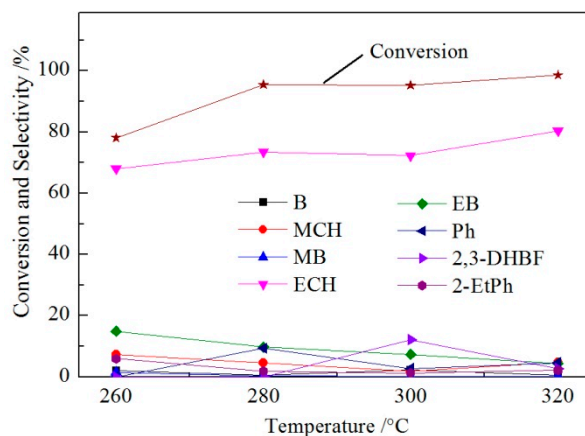


**Figure 8.** Conversion and product distribution of  $\text{Ni}_5\text{Cu}_5/\gamma\text{-Al}_2\text{O}_3$  catalyst with the reaction temperature. (Reaction conditions:  $T = 260\text{--}320$  °C,  $p = 3.0$  MPa,  $\text{WHSV} = 4.0$   $\text{h}^{-1}$ , and hydrogen/oil ratio = 500 (V/V)).

The product distribution of the  $\text{Ni}_5\text{Cu}_5/\gamma\text{-Al}_2\text{O}_3$  catalyst with time on stream is shown in Figure S2. ECH was the main product and the selectivity to ECH increased and reached 72.3% at 8 h. With an extended reaction time, the selectivity to 2,3-DHBF increased initially, reached a maximum, and decreased to 11.2%, whereas the selectivity to EB (which ranged from 7.8%–11.0%) showed little change with reaction time. The selectivity to Ph decreased gradually from ~10% and tended to zero at 8 h. The content of decarbonylated products (B, MB, MCH) could be neglected because of their low selectivities.

### 3. Experimental

#### 3.1. Materials and Preparation of Catalysts

A series of  $\text{Ni-Cu}/\gamma\text{-Al}_2\text{O}_3$  catalysts with different Ni/Cu mass ratios were prepared by impregnation with Nickel nitrate hexahydrate ( $\text{Ni}(\text{NO}_3)_2 \cdot 6\text{H}_2\text{O}$ , 98%) and Copper nitrate trihydrate ( $\text{Cu}(\text{NO}_3)_2 \cdot 3\text{H}_2\text{O}$ , 99.5%). Prior to impregnation, the  $\text{Al}_2\text{O}_3$  support was obtained via calcination of  $\text{AlOOH}$  at 550 °C for 3 h and the  $\text{AlOOH}$  was purchased from Zibo Jiarun Chemical Co., Ltd (Zibo, Shandong, China). The calculated amounts of  $\text{Ni}(\text{NO}_3)_2 \cdot 6\text{H}_2\text{O}$  and  $\text{Cu}(\text{NO}_3)_2 \cdot 3\text{H}_2\text{O}$  were dissolved in distilled water, then the treated  $\gamma\text{-Al}_2\text{O}_3$  support was added into the homogeneous solution. After stirring for 30 min, the suspension was aged for 12 h at room temperature and subsequently dried at 90 °C overnight before being calcined at 500 °C for 3 h. The as-prepared catalysts were denoted as  $\text{Ni}_x\text{Cu}_{(10-x)}/\gamma\text{-Al}_2\text{O}_3$  ( $x = 0, 3, 5, 7, 10$ ), where  $x$  is the mass fraction of Ni and the total metal (both Ni and Cu) loading was fixed at 10 wt.%.

#### 3.2. Characterization

The X-ray diffraction (XRD) analyses were carried out on a D/max-2200PC-X-ray diffractometer (Rigaku, Tokyo, Japan) using  $\text{CuK}\alpha$  radiation under the setting conditions of 40 kV, 30mA, scan range from 10 to 80° at a rate of 10°/min.

The typical physico-chemical properties of supports and catalysts were analyzed by BET method using Micromeritics (Norcross, GA, USA) adsorption equipment of Tristar II 3020. All samples were

outgassed at 200 °C until the vacuum pressure was 6 mm Hg. The adsorption isotherms for nitrogen were measured at −196 °C.

The reducibility of precursors was characterized by the H<sub>2</sub> temperature-programmed reduction (H<sub>2</sub>-TPR) using a quartz U tube reactor (inner diameter of 6 mm), in which 100 mg of samples were loaded in the thermostatic zone. Reduction was conducted from 50 to 800 °C at a heating rate of 10 °C min<sup>−1</sup> in a 10 vol.% H<sub>2</sub>/Ar flow (30 mL min<sup>−1</sup>). The TPR spectrum was determined using a thermal conductivity detector (TCD) to monitor hydrogen consumption.

The X-ray photoelectron spectroscopy (XPS) spectra were acquired using ESCALAB MKII spectrometer (VG, Waltham, MA, USA) under vacuum. XPS measurements have been performed for Mg radiation (E = 1253.6 eV) and equipped with a hemi-spherical analyzer operating at fixed pass energy of 40 eV. The recorded photoelectron binding energies were referenced against the C 1s contamination line at 284.8 eV.

Transmission electron microscope (TEM) examinations were performed using the JEM-1010 instrument supplied by JEOL (Tokyo, Japan). The samples were dispersed in ethanol and placed on a carbon grid before TEM examinations.

The Ni and Cu content was measured by inductively coupled plasma mass spectrometry (ICP-MS) using a Perkin Elmer Nexion 300 instrument (Waltham, MA, USA). Prior to analysis, the sample was digested with nitric acid using microwave heating system.

### 3.3. HDO Performance test

Catalyst testing was conducted in a continuous fixed-bed reactor (8 mm in diameter, 400 mm in length), using a feed of decalin solution of BF (2 wt.%). The conditions of the HDO reaction were 300 °C, 3.0 MPa, WHSV = 4h<sup>−1</sup>, and hydrogen/oil ratio of 500 (V/V). The activities of each catalyst were measured at different time on stream. The feed and reaction product was analyzed by FID gas chromatography (Shimadzu GC-14C, Tokyo, Japan) with a HP-5MS capillary column (length: 30 m, inside diameter: 0.25 mm, film thickness: 0.25 μm).

The BF conversion was calculated from the ratio of converted BF to initial BF using Equation (1):

$$X_{\text{BF}} = \frac{n_{\text{BF},0} - n_{\text{BF},1}}{n_{\text{BF},0}} \times 100\% \quad (1)$$

The selectivity to product *i* was calculated from the ratio of mole amount of product *i* to total product amount and identified as Equation (2):

$$S_i = \frac{n_i}{\sum n_i} \times 100\% \quad (2)$$

The total deoxygenated product yield was defined as the content of all the hydrocarbons via Equation (3):

$$Y_{\text{HDO}} = X_{\text{BF}} \times \frac{\sum n_{\text{hydrocarbon}}}{\sum n_i} \times 100\% \quad (3)$$

where  $n_{\text{BF},0}$  and  $n_{\text{BF},1}$  mean the moles of BF in the feed and product, respectively,  $n_i$  is the mole of product *i*, and  $n_{\text{hydrocarbon}}$  expresses the moles of all the hydrocarbons in the product.

## 4. Conclusions

A series of bimetallic Ni<sub>x</sub>Cu<sub>(10−x)</sub>/γ-Al<sub>2</sub>O<sub>3</sub> catalysts with different Ni/Cu mass ratios was prepared and the effect of the Ni/Cu mass ratio on the BF HDO performance of as-prepared Ni<sub>x</sub>Cu<sub>(10−x)</sub>/γ-Al<sub>2</sub>O<sub>3</sub> catalysts was studied. The interaction between CuO and NiO species over Ni<sub>x</sub>Cu<sub>(10−x)</sub>/γ-Al<sub>2</sub>O<sub>3</sub> catalysts led to smaller and highly dispersed CuO and NiO species over γ-Al<sub>2</sub>O<sub>3</sub>. Compared with monometallic Ni/γ-Al<sub>2</sub>O<sub>3</sub> (130 m<sup>2</sup>·g<sup>−1</sup>) and Cu/γ-Al<sub>2</sub>O<sub>3</sub> (139 m<sup>2</sup>·g<sup>−1</sup>), the Cu-doped bimetallic catalysts showed a higher specific surface area, especially for Ni<sub>5</sub>Cu<sub>5</sub>/γ-Al<sub>2</sub>O<sub>3</sub> (153 m<sup>2</sup>·g<sup>−1</sup>) and Ni<sub>3</sub>Cu<sub>7</sub>/γ-Al<sub>2</sub>O<sub>3</sub>

( $151 \text{ m}^2 \cdot \text{g}^{-1}$ ). All Cu-doped catalysts (monometallic Cu/ $\gamma$ -Al<sub>2</sub>O<sub>3</sub> and bimetallic Ni-Cu/ $\gamma$ -Al<sub>2</sub>O<sub>3</sub>) showed excellent catalytic activities (> 94.5%), which were higher than that of Ni/ $\gamma$ -Al<sub>2</sub>O<sub>3</sub> and indicates that Cu addition can increase the BF HDO activity. Among the as-prepared catalysts, the Ni<sub>5</sub>Cu<sub>5</sub>/ $\gamma$ -Al<sub>2</sub>O<sub>3</sub> showed the highest deoxygenated product yield (79.9%) with an acceptable BF conversion of 95.2%, which increased by 18.3% and 16.9% compared with those of the monometallic Ni/ $\gamma$ -Al<sub>2</sub>O<sub>3</sub> catalyst. The excellent HDO performance of the Ni<sub>5</sub>Cu<sub>5</sub>/ $\gamma$ -Al<sub>2</sub>O<sub>3</sub> catalyst can be attributed to the strong interaction of Ni and Cu. Cu introduction promoted the reduction of nickel oxides and metal-particle dispersion, which improved the catalytic activity. The XPS analysis revealed the electron transfer from Ni to Cu in the bimetallic Ni-Cu/ $\gamma$ -Al<sub>2</sub>O<sub>3</sub> catalysts, which accelerated the C–O bond cleavage, and contributed to oxygen removal. A possible reaction network was proposed, which could provide insight into the BF HDO over a Ni<sub>5</sub>Cu<sub>5</sub>/ $\gamma$ -Al<sub>2</sub>O<sub>3</sub> catalyst.

**Supplementary Materials:** The following are available online at <http://www.mdpi.com/2073-4344/10/3/274/s1>, Figure S1: Total deoxygenated product yield of Ni<sub>x</sub>Cu<sub>(10-x)</sub>/ $\gamma$ -Al<sub>2</sub>O<sub>3</sub> catalysts at 8 h; Figure S2: Production distribution of Ni<sub>5</sub>Cu<sub>5</sub>/ $\gamma$ -Al<sub>2</sub>O<sub>3</sub> catalyst with the reaction time on stream.

**Author Contributions:** T.Z. carried out the catalyst preparation and experimental tests and wrote the draft of the manuscript. H.S. designed the experiment and analyzed the data; F.L. and Y.C. reviewed and edited the manuscript. All authors have read and agreed to the published version of the manuscript.

**Funding:** This research received no external funding

**Acknowledgments:** This work was supported by the Graduate Innovation Project of Northeast Petroleum University (JYCX\_CX03\_2018).

**Conflicts of Interest:** The authors declare no conflict of interest.

## References

1. Gollakota, A.R.K.; Reddy, M.; Subramanyam, M.D.; Kishore, N. A review on the upgradation techniques of pyrolysis oil. *Renew. Sust. Energy Rev.* **2016**, *58*, 1543–1568. [[CrossRef](#)]
2. Wang, H.; Male, J.; Wang, Y. Recent advances in hydrotreating of pyrolysis bio-oil and its oxygen-containing model compounds. *ACS Catal.* **2013**, *3*, 1047–1070. [[CrossRef](#)]
3. Huber, G.W.; O'Connor, P.; Corma, A. Processing biomass in conventional oil refineries: Production of high quality diesel by hydrotreating vegetable oils in heavy vacuum oil mixtures. *Appl. Catal. A Gen.* **2007**, *329*, 120–129. [[CrossRef](#)]
4. Yildiz, G.; Pronk, M.; Djokic, M.; van Geem, K.M.; Ronsse, F.; van Duren, R.; Prins, W. Validation of a new set-up for continuous catalytic fast pyrolysis of biomass coupled with vapour phase upgrading. *J. Anal. Appl. Pyrol.* **2013**, *103*, 343–351. [[CrossRef](#)]
5. Prajitno, H.; Insyani, R.; Park, J.; Ryu, C.; Kim, J. Non-catalytic upgrading of fast pyrolysis bio-oil in supercritical ethanol and combustion behavior of the upgraded oil. *Appl. Energy* **2016**, *172*, 12–22. [[CrossRef](#)]
6. Romero, Y.; Richard, F.; Brunet, S. Hydrodeoxygenation of 2-ethylphenol as a model compound of bio-crude over sulfided Mo-based catalysts: Promoting effect and reaction mechanism. *Appl. Catal. B Environ.* **2010**, *98*, 213–223. [[CrossRef](#)]
7. Brillouet, S.; Baltag, E.; Brunet, S.; Richard, F. Deoxygenation of decanoic acid and its main intermediates over unpromoted and promoted sulfided catalysts. *Appl. Catal. B Environ.* **2014**, *148*, 201–211. [[CrossRef](#)]
8. Gonçalves, V.O.O.; Brunet, S.; Richard, F. Hydrodeoxygenation of cresols over Mo/Al<sub>2</sub>O<sub>3</sub> and CoMo/Al<sub>2</sub>O<sub>3</sub> sulfided catalysts. *Catal. Lett.* **2016**, *146*, 1562–1573. [[CrossRef](#)]
9. Şenol, O.İ.; Viljava, T.R.; Krause, A.O.I. Effect of sulphiding agents on the hydrodeoxygenation of aliphatic esters on sulphided catalysts. *Appl. Catal. A Gen.* **2007**, *326*, 236–244. [[CrossRef](#)]
10. Nie, L.; Resasco, D.E. Kinetics and mechanism of m-cresol hydrodeoxygenation on a Pt/SiO<sub>2</sub> catalyst. *J. Catal.* **2014**, *317*, 22–29. [[CrossRef](#)]
11. De Souza, P.M.; Rabelo-Neto, R.C.; Borges, L.E.P.; Jacobs, G.; Davis, B.H.; Sooknoi, T.; Resasco, D.E.; Noronha, F.B. Role of keto intermediates in the hydrodeoxygenation of phenol over Pd on oxophilic supports. *ACS Catal.* **2015**, *5*, 1318–1329. [[CrossRef](#)]

12. Newman, C.; Zhou, X.; Goundie, B.; Ghampson, I.T.; Pollock, R.A.; Ross, Z.; Wheeler, M.C.; Meulenberg, R.W.; Austin, R.N.; Frederick, B.G. Effects of support identity and metal dispersion in supported ruthenium hydrodeoxygenation catalysts. *Appl. Catal. A Gen.* **2014**, *477*, 64–74. [[CrossRef](#)]
13. Zhou, M.; Ye, J.; Liu, P.; Xu, J.; Jiang, J. Water-assisted selective hydrodeoxygenation of guaiacol to cyclohexanol over supported Ni and Co bimetallic catalysts. *ACS Sustain. Chem. Eng.* **2017**, *5*, 8824–8835. [[CrossRef](#)]
14. Leng, S.; Wang, X.; He, X.; Liu, L.; Liu, Y.; Zhong, X.; Zhuang, G.; Wang, J. NiFe/ $\gamma$ -Al<sub>2</sub>O<sub>3</sub>: A universal catalyst for the hydrodeoxygenation of bio-oil and its model compounds. *Catal. Commun.* **2013**, *41*, 34–37. [[CrossRef](#)]
15. Cheng, S.; Wei, L.; Julson, J.; Rabnawaz, M. Upgrading pyrolysis bio-oil through hydrodeoxygenation (HDO) using non-sulfided Fe-Co/SiO<sub>2</sub> catalyst. *Energy Convers. Manag.* **2017**, *150*, 331–342. [[CrossRef](#)]
16. Carrero, A.; Calles, J.A.; García-Moreno, L.; Vizcaino, A.J. Production of renewable hydrogen from glycerol steam reforming over bimetallic Ni-(Cu, Co, Cr) catalysts supported on SBA-15 Silica. *Catalysts* **2017**, *7*, 55. [[CrossRef](#)]
17. Tuan, L.A.; Luong, N.T.; Ishihara, K.N. Low-temperature catalytic performance of Ni-Cu/Al<sub>2</sub>O<sub>3</sub> catalysts for gasoline reforming to produce hydrogen applied in spark ignition engines. *Catalysts* **2016**, *6*, 45. [[CrossRef](#)]
18. Berenguer, A.; Sankaranarayanan, T.M.; Gómez, G.; Moreno, I.; Coronado, J.M.; Pizarro, P.; Serrano, D.P. Evaluation of transition metal phosphides supported on ordered mesoporous materials as catalysts for phenol hydrodeoxygenation. *Green Chem.* **2016**, *18*, 1938–1951. [[CrossRef](#)]
19. Sutton, A.D.; Waldie, F.D.; Wu, R.; Schlaf, M.; Silks, L.A.; Gordon, J.C. The hydrodeoxygenation of bioderived furans into alkanes. *Nat. Chem.* **2013**, *5*, 428–432. [[CrossRef](#)]
20. Liu, R.; Pang, M.; Chen, X.; Li, C.; Xu, C.; Liang, C. W<sub>2</sub>C nanorods with various amounts of vacancy defects: Determination of catalytic active sites in the hydrodeoxygenation of benzofuran. *Catal. Sci. Technol.* **2017**, *7*, 1333–1341. [[CrossRef](#)]
21. Bunch, A.Y.; Ozkan, U.S. Investigation of the reaction network of benzofuran hydrodeoxygenation over sulfided and reduced Ni-Mo/Al<sub>2</sub>O<sub>3</sub> catalysts. *J. Catal.* **2002**, *206*, 177–187. [[CrossRef](#)]
22. Chen, S.; Zhou, G.; Xie, H.; Jiao, Z.; Zhang, X. Hydrodeoxygenation of methyl laurate over the sulfur-free Ni/ $\gamma$ -Al<sub>2</sub>O<sub>3</sub> catalysts. *Appl. Catal. A Gen.* **2019**, *569*, 35–44. [[CrossRef](#)]
23. Ham, H.; Baek, S.W.; Shin, C.H.; Bae, J.W. Roles of Structural Promoters for Direct CO<sub>2</sub> Hydrogenation to Dimethyl Ether over Ordered Mesoporous Bifunctional Cu/M-Al<sub>2</sub>O<sub>3</sub> (M = Ga or Zn). *ACS Catal.* **2018**, *9*, 679–690. [[CrossRef](#)]
24. Cai, F.; Pan, D.; Ibrahim, J.J.; Zhang, J.; Xiao, G. Hydrogenolysis of glycerol over supported bimetallic Ni/Cu catalysts with and without external hydrogen addition in a fixed-bed flow reactor. *Appl. Catal. A Gen.* **2018**, *564*, 172–182. [[CrossRef](#)]
25. Hou, Z.; Yokota, O.; Tanaka, T.; Yashima, T. Characterization of Ca-promoted Ni/ $\alpha$ -Al<sub>2</sub>O<sub>3</sub> catalyst for CH<sub>4</sub> reforming with CO<sub>2</sub>. *Appl. Catal. A Gen.* **2003**, *253*, 381–387. [[CrossRef](#)]
26. Nie, R.; Yang, H.; Zhang, H.; Yu, X.; Lu, X.; Zhou, D.; Xia, Q. Mild-temperature hydrodeoxygenation of vanillin over porous nitrogen-doped carbon black supported nickel nanoparticles. *Green Chem.* **2017**, *19*, 3126–3134. [[CrossRef](#)]
27. Liu, L.; Lou, H.; Chen, M. Selective hydrogenation of furfural to tetrahydrofurfuryl alcohol over Ni/CNTs and bimetallic Cu-Ni/CNTs catalysts. *Int. J. Hydrogen Energy* **2016**, *41*, 1721–14731. [[CrossRef](#)]
28. Xin, J.; Cui, H.; Cheng, Z.; Zhou, Z. Bimetallic Ni-Co/SBA-15 catalysts prepared by urea co-precipitation for dry reforming of methane. *Appl. Catal. A Gen.* **2018**, *554*, 95–104. [[CrossRef](#)]
29. Ambursa, M.M.; Ali, T.H.; Lee, H.V.; Sudarsanam, P.; Bhargava, S.K.; Hamid, S.B.A. Hydrodeoxygenation of dibenzofuran to bicyclic hydrocarbons using bimetallic Cu-Ni catalysts supported on metal oxides. *Fuel* **2016**, *180*, 767–776. [[CrossRef](#)]
30. Yang, F.; Liu, D.; Zhao, Y.; Wang, H.; Han, J.; Ge, Q.; Zhu, X. Size dependence of vapor phase hydrodeoxygenation of m-cresol on Ni/SiO<sub>2</sub> catalysts. *ACS Catal.* **2018**, *8*, 1672–1682. [[CrossRef](#)]
31. Resasco, D.E. What should we demand from the catalysts responsible for upgrading biomass pyrolysis oil? *J. Phys. Chem. Lett.* **2011**, *2*, 2294–2295. [[CrossRef](#)]
32. Song, H.; Gong, J.; Song, H.; Li, F. A novel surface modification approach for synthesizing supported nickel phosphide catalysts with high activity for hydrodeoxygenation of benzofuran. *Appl. Catal. A Gen.* **2015**, *505*, 267–275. [[CrossRef](#)]
33. Zhu, T.; Song, H.; Dai, X.; Song, H. Preparation of Ni<sub>2</sub>P/Al-SBA-15 catalyst and its performance for benzofuran hydrodeoxygenation. *Chin. J. Chem. Eng.* **2017**, *25*, 1784–1790. [[CrossRef](#)]

34. Iino, A.; Cho, A.; Takagaki, A.; Kikuchi, R.; Oyama, S.T. Kinetic studies of hydrodeoxygenation of 2-methyltetrahydrofuran on a Ni<sub>2</sub>P/SiO<sub>2</sub> catalyst at medium pressure. *J. Catal.* **2014**, *311*, 17–27. [[CrossRef](#)]
35. Jiang, B.; Zhu, T.; Song, H.; Li, F. Hydrodeoxygenation and hydrodesulfurization over Fe promoted Ni<sub>2</sub>P/SBA-15 catalyst. *J. Alloys Compd.* **2019**, *806*, 254–262. [[CrossRef](#)]



© 2020 by the authors. Licensee MDPI, Basel, Switzerland. This article is an open access article distributed under the terms and conditions of the Creative Commons Attribution (CC BY) license (<http://creativecommons.org/licenses/by/4.0/>).